Horse cyt. *c* is a highly basic protein with a pI close to 10, where the charge state of the protein at pH 7 is +8. Association of **1**, an octaanionic species near neutral pH, leads to a major disruption of the coulombic interactions between the surface lysine residues and other regions of the protein with likely destabilization of the folded structure. In a related way, partial acetylation of the lysine (see above)[17] and binding to acidic lipid membranes[24] leads to a disruption of electrostatic surface potential and a similar destabilization of cyt. *c*. However, interaction with the denatured state may make an equally significant contribution to the effect of **1**.[25, 26] In order to probe the interaction of **1** with the denatured state, we carried out a fluorescence quenching titration at higher temperatures. At 75 °C, the fluorescence of **1** is completely quenched by addition of approximately 0.33 equivalents of cyt. *c*. This indicates binding of at least 3 equivalents of **1** to the unfolded form of the protein, which would be expected to have a larger accessible hydrophobic surface area than the native conformation.[27]

Compound **1** takes advantage of complementary hydrophobic and electrostatic interactions to achieve high affinity and selectivity. Like other destabilizers,[5] **1** appears to act through destabilizion of the native state in addition to the stabilization of the unfolded state. However, in the case of **1**, increased selectivity and efficacy is achieved through strong affinity to both states, inducing unfolding at much lower concentrations. This strategy offers a potentially general approach to designing molecules that denature other globular proteins with potency and selectivity.

Received: November 2, 2001 [Z18149]

[1] B. A. Foster, H. A. Coffey, M. J. Morin, F. Rastinejad, *Science* **1999**, *286*, 2507 – 2510.
[2] J. R. Peterson, R. S. Lokey, T. J. Mitchison, M. W. Kirschner, *Proc. Natl. Acad. Sci. USA* **2001**, *98*, 10624 – 10629.
[3] For an example of selective disruption of protein quaternary structure, see: D. K. Leung, Z. Yang, R. Breslow, *Proc. Natl. Acad. Sci. USA* **2000**, *97*, 5050 – 5053.
[4] C. Tanford, *Adv. Protein Chem.* **1968**, *14*, 121 – 244.
[5] S. N. Timasheff, *Biochemistry* **1992**, *31*, 9857 – 9864.
[6] T. J. T. Pinheiro, H. Cheng, S. H. Seeholzer, H. Roder, *J. Mol. Biol.* **2000**, *303*, 617 – 626.
[7] T. K. Das, S. Mazumdar, S. Mitra, *Eur. J. Biochem.* **1998**, *254*, 662 – 670.
[8] G. C. Kresheck, J. E. Erman, *Biochemistry* **1988**, *27*, 2490 – 2496.
[9] C. A. Yu, S. H. Gwak, L. Yu, *Biochim. Biophys. Acta* **1985**, *812*, 656 – 664.
[10] H. Pelletier, J. Kraut, *Science* **1992**, *258*, 1748 – 1755.
[11] R. K. Jain, A. D. Hamilton, *Org. Lett.* **2000**, *2*, 1721 – 1723.
[12] C. O. Fagain, *Biochim. Biophys. Acta* **1995**, *1252*, 1 – 14.
[13] R. Lumry, E. Eyring, *J. Phys. Chem.* **1954**, *58*, 110 – 120.
[14] J. M. Sanchez-Ruiz, *Biophys. J.* **1992**, *61*, 921 – 935.
[15] V. Edge, N. M. Allewell, J. M. Sturtevant, *Biochemistry* **1985**, *24*, 5899 – 5906.
[16] Porphyrin **2** shows no binding to cyt. *c* under these conditions.[10]
[17] Y. Hagihara, Y. Tan, Y. Goto, *J. Mol. Biol.* **1994**, *237*, 336 – 348.
[18] Y. Matsuura, T. Takano, R. E. Dickerson, *J. Mol. Biol.* **1982**, *156*, 389 – 409.
[19] A. Wada, H. Nakamura, *Nature* **1981**, *293*, 757 – 758.
[20] A. Karshikoff, R. Ladenstein, *Protein Eng.* **1988**, *11*, 867 – 872.
[21] L. Xiao, B. Honig, *J. Mol. Biol.* **2000**, *289*, 1435 – 1444.
[22] C. N. Pace, *Nat. Struct. Biol.* **2000**, *7*, 345 – 346.
[23] D. Perl, U. Mueller, U. Heinemann, F. X. Schmid, *Nat. Struct. Biol.* **2000**, *7*, 380 – 383.
[24] A. Muga, H. H. Mantsch, W. K. Surewicz, *Biochemistry* **1991**, *30*, 7219 – 7224.
[25] D. Shortle, *FASEB J.* **1996**, *10*, 27 – 34.
[26] T. Arakawa, S. J. Prestrelski, W. C. Kenney, J. F. Carpenter, *Adv. Drug Delivery Rev.* **2001**, *46*, 307 – 326.
[27] Y. Hagihara, M. Hoshino, D. Hamada, M. Kataoka, Y. Goto, *Folding Des.* **1998**, *3*, 195 – 201.

Synthesis and Characterization of Ag_2NiO_2 Showing an Uncommon Charge Distribution**

Martin Schreyer and Martin Jansen*

The unique structural features of silver-rich silver(I) oxides were the earliest experimental evidence suggesting attractive $d^{10}-d^{10}$ interactions between monovalent silver atoms.[1, 2] In spite of bearing equal positive charges, the silver atoms in these compounds interconnect forming cluster-like ensembles corresponding to sections of the element structure of silver. Those structural features are accompanied by the formation of an empty band of mainly Ag-5s character near the Fermi level, capable of accommodating additional electrons. Consequently, silver is expected to adopt subvalent valence states in solid materials.[3] Only a few examples such as, Ag_2F,[4] Ag_3O,[5] Ag_5SiO_4,[6, 7] Ag_5GeO_4,[6, 8] and $Ag_5Pb_2O_6$[9] have been prepared to date. The properties range from metallic behavior in Ag_2F, Ag_3O, and $Ag_5Pb_2O_6$ to semiconducting in Ag_5SiO_4 and Ag_5GeO_4.

Surprisingly, the new silveroxonickelate Ag_2NiO_2 also contains subvalent silver. Conventionally, the oxidation states +1 and +2 would be assigned to silver and nickel, respectively, which correspond to the valence distribution in the homologous compound Ag_2PdO_2.[10] These assignments, however, severely conflict with the structural features, magnetic moment, and spectroscopic properties found in Ag_2NiO_2. Instead, all the experimental findings are consistent with a charge distribution of $[Ag_2]^+[NiO_2]^-$.

Ag_2NiO_2 has been prepared by the solid-state reaction of Ag_2O and NiO under high oxygen pressure. Ag_2NiO_2 is a lustrous black solid and insensitive to air and water. The crystal structure has been determined and refined from X-ray and neutron powder data, and from single-crystal X-ray data.[11] There are striking similarities with the delafossite structure[12] on the one hand as well as with the silver suboxide Ag_3O[5] and the silver subfluoride Ag_2F,[4] on the other.

[*] Prof. Dr. M. Jansen, Dr. M. Schreyer
Max-Planck-Institut für Festköperforschung
Heisenbergstrasse 1
70569 Stuttgart (Germany)
Fax: (+49) 711-689-1502
E-mail: M.Jansen@fkf.mpg.de

[**] The authors gratefully acknowledge preliminary synthetic work by Norbert Priesmann. We thank Dr. Hartwig Modrow for providing the XANES-results obtained in the ELSA SR-laboratory and Dr. Ulrich Wedig for performing the Hartree – Fock calculations. Also, we thank Eva Bruecher, Gisela Siegle, and Dr. Reinhard K. Kremer for determining the electric and magnetic properties of the material.

Figure 1 compares the structure of Ag_2NiO_2 with the structure of the delafossite $AgNiO_2$[13] and silver subfluoride. In delafossites of the composition $AgMO_2$ (M = trivalent transition metal ion),[12] MO_6 octahedra are linked by their edges to form cadmium chloride analogous layers. These layers are interconnected by linear O-Ag-O bridges and stacked along

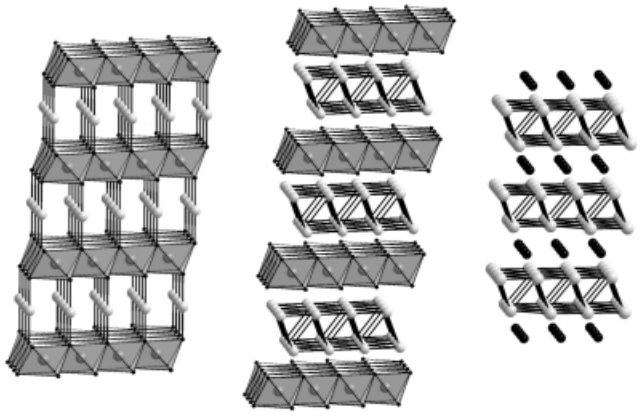

Figure 1. Comparison of the crystal structures of $AgNiO_2$ (left), Ag_2NiO_2 (center), and Ag_2F (right); silver: white, nickel: dark gray, fluorine: black.

the *c* axis (Figure 1) giving either the H- or R-polytype of the delafossite structure. Like $AgNiO_2$, which represents the R-polytype, Ag_2NiO_2 also crystallizes in the trigonal space group $R\bar{3}2/m$ (No. 166). Compared to $AgNiO_2$ the *a* axis is slightly reduced from 2.9390(1) to 2.926(1) Å while the *c* axis is considerably elongated from 18.3700(1) to 24.0888(2) Å. The geometry of the cadmium-chloride-like NiO_2 layers remains virtually unchanged in Ag_2NiO_2 (Table 1). However,

Table 1. Distances [Å] and angles [°] in Ag_2NiO_2 and, for comparison, in $AgNiO_2$,[13] Ag_2F,[4] and Ag_3O.[5]

	Ag_2NiO_2	$AgNiO_2$[13]	Ag_2F[4]	Ag_3O[5]
Ni-O	1.976(1)(×6)	1.94(×6)	–	–
Ag-O/Ag-F	2.506(1)(×3)	2.12(×2)	2.451(×3)	2.292(1)
Ag-Ag in plane	2.926(1)(×6)	2.939(×6)	2.996(×6)	3.074(1)[a]
Ag-Ag vertical	2.836(1)(×3)		2.814(×3)	2.833(1)[a]
O-Ni-O (1)	95.53(1)	98.50	–	–
O-Ni-O (2)	84.47(1)	81.50	–	–

[a] Mean distances.

the NiO_2 slabs are now separated by two staggered hexagonal silver layers. Thus, silver is coordinated by three oxygen atoms forming the basis of a trigonal pyramid with the silver atom at its top. This feature corresponds to the silver substructure of Ag_2F where the silver atoms also form layers of edge-sharing octahedra. As shown in Table 1, silver–silver and silver–anion distances are in good agreement with those in the silver subfluoride. Thus, $[Ag_2]^+$ and $[NiO_2]^-$ slabs alternate with each other, to form the structure of Ag_2NiO_2. The in-plane silver–silver distances are 2.926(1) Å and thus similar to those in elementary silver (2.889 Å). The smallest distances between adjacent silver atoms of subsequent layers are even shorter at 2.836(1) Å. Since this short distance is not enforced by structural constraints, it must be directly attributed to chemical bonds between the silver atoms. This proposal suggests that in Ag_2NiO_2 there is classic metallic Ag–Ag bonding mediated by an additional valence electron per two silver atoms, in addition to the $d^{10}-d^{10}$ interactions effective in the R-delafossites. As there is only one crystallographic silver position and silver has an oxidation state of +1/2, at least partial metallic character can be attributed to this bond. Once again this is supported by the comparison with silver subfluoride Ag_2F and Ag_3O silver suboxide which are both metallic conductors.

These assignments of valence states are conclusively confirmed by the physical and spectroscopic properties of Ag_2NiO_2. First, Ag_2NiO_2 is a good metallic conductor with a specific resistance of $2.18 \times 10^{-4}\ \Omega$ cm at 298 K and a positive temperature coefficient (Figure 2) of 70.78 $\mu\Omega\,cm\,K^{-1}$. This

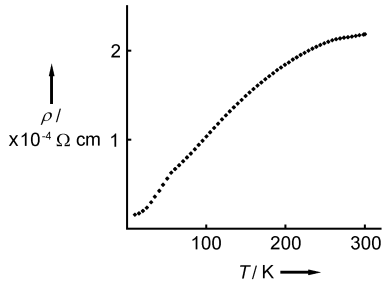

Figure 2. Temperature dependence of the electrical resistivity of Ag_2NiO_2.

situation is comparable to the electric transport properties of Ag_2F and Ag_3O. Second, Ag_2NiO_2 is an antiferromagnet with $T_N = 56$ K and a Weiss temperature of 32 K (Figure 3). The magnetic moment as derived from the susceptibility data of the paramagnetic Curie–Weiss region above 56 K amounts to $\mu = 1.95\ \mu_b$, which corresponds to Ni^{3+} center in a low spin state. At 250 K a slight baseline shift in the inverse magnetic susceptibility is observed that may be attributed to a change in the itinerant valence-electron concentration. However, a conclusive explanation of this latter features requires further investigation.

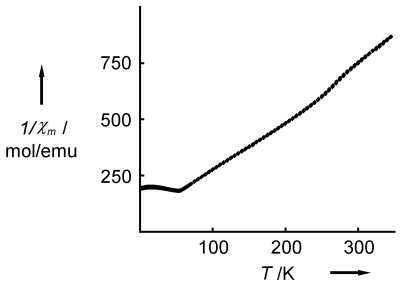

Figure 3. Temperature characteristic of the inverse molar susceptibility of Ag_2NiO_2.

The valence states of silver and nickel were experimentally investigated by XANES-spectroscopy (Figure 4). With an increasing nickel oxidation state, the absorption edge is shifted to higher energies. Particularly, the absorption edges of Ag_2NiO_2 and $AgNiO_2$ coincide largely with respect to shape, turning points and band positions which indicates equal valence states for nickel in both compounds. Also, a compar-

  1433-7851/02/4104-0644 $ 17.50+.50/0 *Angew. Chem. Int. Ed.* **2002**, *41*, No. 4

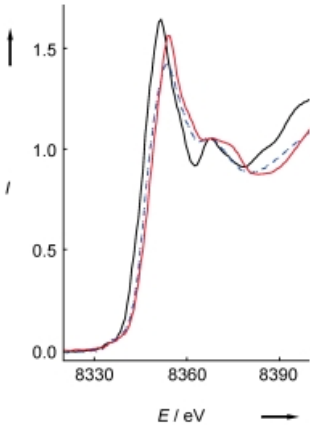

Figure 4. Ni-K-Edge-XANES-Spectra of Ag_2NiO_2 (blue broken line), $AgNiO_2$ (red solid line), and NiO (black solid line).

ison of the Ag-L_3-XANES-spectra of Ag_2O, $AgNiO_2$, and Ag_2NiO_2 (Figure 5), lends strong support to the valence distribution suggested for Ag_2NiO_2. Two different features of the spectra are to be considered. Firstly, the position of the absorption edge is related to the binding energy of the silver L-shell electrons which is expected to diminish with decreasing silver oxidation state. In Ag_2NiO_2 the absorption edge is significantly shifted to lower energy in comparison to Ag_2O and $AgNiO_2$. This can be stated although the true position of the absorption edges in the latter two compounds is obscured by the pre-edge absorption edge, an effect that increasingly shifts the absorption edge to lower energies. Secondly, the peak areas below the pre-edge absorption peaks correlate with the number of empty d-band states. These empty states are of significant magnitude for $AgNiO_2$ and Ag_2O and are virtually completely filled for Ag_2NiO_2.[14]

The peculiar valence-state distribution in Ag_2NiO_2 can be interpreted in terms of a stronger ligand-field stabilization of low-spin Ni^{3+} compared to Ni^{2+} centers in octahedral coordination and of low-lying silver 5s and 5p bands capable of accommodating excess electron density. The density of states (DOS) obtained for Ag_2F and Ag_2NiO_2 at the Hartree–Fock (HF) level show similar characteristics (Figure 6). Those parts of the DOS projected onto the 4d orbitals of silver are situated well below the Fermi level. The same is true for Ni-3d and O-3p contributions. The energy range around the Fermi level is characterized by the presence of rather dispersed bands which predominantly correspond to Ag-5s/5p states. In this respect, the DOS and their projections in Ag_2NiO_2 closely resemble those in Ag_2F.

All current experimental and theoretical evidence leads to the conclusion that the new ternary silveroxonickelate Ag_2NiO_2 has an unexpected and unprecedented charge distribution. In particular, the presence of subvalent silver ($Ag^{1/2+}$) next to rather highly oxidized nickel (Ni^{3+}) center appears puzzling and resembles a short-circuited solid-state battery.

Experimental Section

Ag_2NiO_2 was formed by a solid-state reaction from a ground mixture of Ag_2O and NiO in the molar proportion 1.05:1 by annealing at 823 K under an oxygen pressure of 65 MPa. A potassium hydroxide solution (1.5 mL; 5 M) was added as a mineralizator, the reaction time was 24 h.

Received: November 26, 2001 [Z 18281]

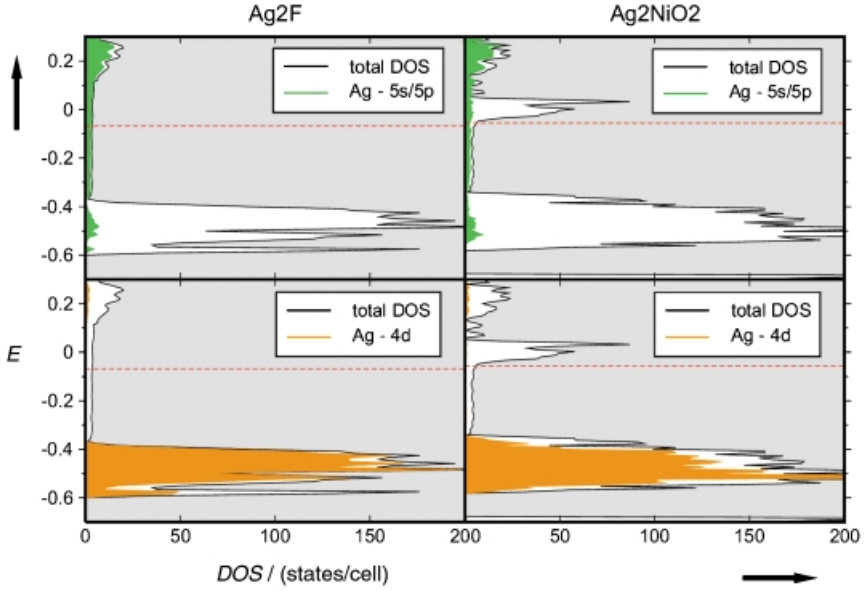

Figure 6. Comparison of the HF-calculated DOS of Ag_2F and Ag_2NiO_2.

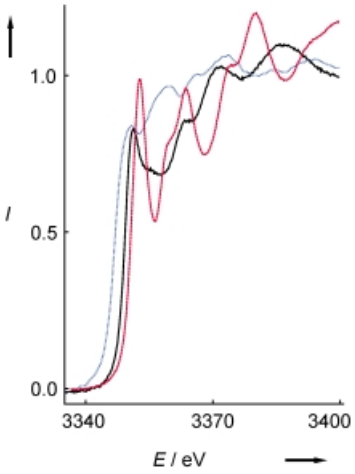

Figure 5. Ag-L_3-edge-XANES spectra of Ag_2NiO_2 (blue broken line), $AgNiO_2$ (red solid line), and (black solid line) Ag_2O.

[1] M. Jansen, Habilitationsschrift, Gießen, **1978**.
[2] M. Jansen, *J. Less-Common Met.* **1980**, *76*, 285.
[3] M. Jansen, *Angew. Chem.* **1987**, *99*, 1136; *Angew. Chem. Int. Ed. Engl.* **1987**, *26*, 1098.
[4] G. Argay, F. Naray-Szabo, *Acta Chim. Acad. Sci. Hung.* **1966**, 329.
[5] W. Beesk, P. G. Jones, H. Rumpel, E. Schwarzmann, G. M. Sheldrick, *J. Chem. Soc. Chem. Commun.* **1981**, 644.
[6] M. Jansen, C. Linke, *Z. Anorg. Allg. Chem.* **1992**, *616*, 95.
[7] C. Linke, M. Jansen, *Inorg. Chem.* **1994**, *33*, 2614.
[8] M. Jansen, C. Linke, *Angew. Chem.* **1992**, *104*, 618; *Angew. Chem. Int. Ed. Engl.* **1992**, *31*, 653.
[9] M. Jansen, M. Bortz, K. Heidebrecht, *Z. Kristallogr.* **1989**, *186*, 147; M. Jansen, M. Bortz, K. Heidebrecht, *J. Less-Common Met.* **1990**, *161*, 17.
[10] M. Schreyer, M. Jansen, *Solid State Sci.* **2001**, *3*, 25.
[11] Structure analysis of Ag_2NiO_2. X-ray powder diffraction: Space group $R\bar{3}m$, $a = 2.92647(2)$, $b = 24.0888(2)$ Å, $V = 178.663$ Å^3, $Z = 3$; Stoe-Stadi-P-transmission powder diffractometer $Cu_{K\alpha 1}$ radiation, linear position sensitive detector (Stoe-mini-PSD), transmission mode, 6009 data points, measurement range: $5° < 2\theta < 125°$, measurement time: 72 h, 57 observed reflections, 2 refined atomic positions, 3 refined

  1433-7851/02/4104-0645 $ 17.50+.50/0

temperature coefficients, Rietveld refinement: R_{wp}: 0.0849, R_{bragg}: 0.0435, GOF: 3.585. Neutron diffraction data: Space group $R\bar{3}m$, $a=2.92471(2)$, $b=24.0746(4)$ Å, $V=178.342(3)$ Å^3, $Z=3$; ROTAX/ISIS, Vanadium tube, time-of-flight (TOF) measurement, 3 detector banks; detector bank A: 1355 data points; detector bank B: 2129 data points; detector bank C: 2016 data points, 1006 observed reflections, 2 refined atomic parameters, 3 refined temperature coefficients, Rietveld refinement: $R_{wp}=0.0283$, $\chi^2=3.619$. Single-crystal X-ray refinement: Space group $R\bar{3}m$, $a=2.9193(4)$, $b=24.031(4)$ Å, $V=177.36(5)$ Å^3, $Z=3$; Bruker AXS Smart CCD 1000, $Mo_{K\alpha}$, measurement range: $2.54^\circ<\theta<34.49^\circ$, 131 reflections, refinement with SHELXL 97-2: $R_1=0.0132$, $R_{wp}=0.0126$, Further details on the crystal structure investigation may be obtained from the Fachinformationszentrum Karlsruhe, 76344 Eggenstein-Leopoldshafen, Germany (fax: (+49) 7247-808-666; e-mail: crysdata@fiz-karlsruhe.de), on quoting the depository number CSD-412279.

[12] A. Pabst, *Am. Mineral.* **1938**, *23*, 175.

[13] A. Wichainchai, P. Dordor, J. P. Doumerc, E. Marquestaut, Mi. Pouchard, P. Hagenmuller, A. Ammar, *J. Solid State Chem.* **1988**, *74*, 126.

[14] M. Schreyer, M. Jansen, U. Wedig, H. Modrow, P. Adler, W. Kockelmann, unpublished results.

A Mass Spectrometry Based Direct-Binding Assay for Screening Binding Partners of Proteins**

Hanfa Zou,* Qingchun Zhang, Zhong Guo, Baochuan Guo, Qiang Zhang, and Xiaoming Chen

Recent advances in genomics and proteomics have enabled the discovery of more drug targets than ever before. The majority of these drug targets are proteins. One of the most challenging areas of drug development is the search for novel receptor–ligand pairs and enzyme inhibitors,[1, 2] as many novel proteins have no known binding partners. During the drug discovery process, the binding partners of a receptor or protein must be found in order to determine possible ways to address its pathological pathway.

Ligand fishing is a widely used process in which proteins are screened against a multitude of compounds to search for the binding partners of the proteins. The most common methods for ligand fishing are those based on direct binding and one of the most versatile direct-binding assays involves the use of biosensors based on surface plasma resonance (SPR).[3–5] However, a major drawback of SPR is that once a sample is identified as having a possible binding partner, other conventional biochemical techniques, for example, HPLC and mass spectrometry,[6] need to be applied to identify the new ligand.

Herein we describe a novel on-probe direct-binding assay to screen the binding partners of a target protein. Contrary to the case in SPR, the captured binding partners in this direct-binding assay are directly analyzed on-probe by means of mass spectrometry. The target protein is first immobilized on a porous silicon probe. A sample that contains possible binding partners is then incubated with the probe, and the binding partners are captured by the immobilized protein. The captured binding partner is then identified by means of on-probe laser desorption/ionization time-of-flight (TOF) mass spectrometric analysis.

Unlike other mass spectrometry based assays in which biologically active probes are used for rapid analyses of a sample,[7–12] this new assay involves desorption/ionization on silicon (DIOS)[13–15] instead of matrix-assisted laser desorption/ionization (MALDI) in the ionization process. The use of DIOS is based on two considerations. First, the majority of the drug candidates are low-mass molecules. In MALDI, the matrix is essential to desorption/ionization, but the use of matrix also generates strong matrix-related background noise in the low-mass region, which obscures or even suppresses the analytical signals of other low-mass molecules. In contrast, a matrix is not required for DIOS and laser desorption/ionization is performed on porous silicon, therefore eliminating the matrix-related background problem. DIOS is very effective for analysis of low-mass molecules. Second, DIOS involves the use of porous silicon as a probe on which proteins can easily be immobilized. Furthermore, the porous silicon probe can be generated routinely through electrochemical anodization[15, 16] or chemical etching[17–19] of flat crystalline silicon. The porous silicon surface can be regenerated easily.

A silicon wafer was galvanostatically etched and oxidized. The preparation of a good porous silicon probe is essential for the success of this assay, as only well-etched silicon wafers produce good ion signals by laser desorption/ionization without the use of matrix. We have a porous silicon probe for the routine generation of good mass spectra of a variety of drugs, including atropine, propanolol, atenolol, alprenolol, metoprolol, warfarin, sulpride, naproxen, and ketoprofen. Figure 1 shows the mass spectrum[20] of naproxen obtained when using a) MALDI with 2,5-dihydroxybenzoic acid (DHB) as matrix and b) the DIOS technique. Clearly, a number of strong matrix-related peaks were present in the mass spectrum when a DHB matrix was used (Figure 1a). In contrast, the only major peak in the DIOS spectrum (Figure 1b) corresponds to naproxen and, importantly, no fragmentation of naproxen was observed in DIOS. We have also been able to produce good mass spectra of a variety of peptides of less than 500 Da by means of DIOS. Furthermore, we have successfully used this method to detect the products of the derivatization of cyclodextrin.

Because many drug molecules are good binding partners of bovine serum albumin (BSA), we tested this new direct binding assay with BSA. BSA was immobilized on the porous silicon probe with 2,4,6-trichloro-1,3,5-triazine as the activated agent. The experimental procedure for the immobilization

[*] Prof. H. Zou, Q. Zhang, Z. Guo, Q. Zhang, X. Chen
National Chromatographic R&A Center
Dalian Institute of Chemical Physics, Chinese Academy of Sciences
Dalian 116011 (China)
Fax: (+86) 411-369-3407
E-mail: zouhfa@mail.dlptt.ln.cn
Prof. B. Guo
Department of Chemistry, Cleveland State University
Cleveland, OH 44115 (USA)

[**] Financial support from the Chinese Academy of Sciences (STZ-00-09) and the Knowledge Innovation Program of DICP to H.Z. are gratefully acknowledged. H.Z. is the recipient of an Excellent Young Scientist Award from the National Natural Science Foundation of China (No.29725512).

  1433-7851/02/4104-0646 $ 17.50+.50/0